

Design of novel organic proton-transfer acid-base (anti-)ferroelectric salts with crystal structure prediction

S. Seyedraoufi,¹ Graeme M. Day,² and Kristian Berland^{1,*}

¹*Department of Mechanical Engineering and Technology Management, Norwegian University of Life Sciences, 1432 Ås, Norway.*

²*School of Chemistry, University of Southampton, Southampton SO17 1BJ, United Kingdom.*

(Dated: October 29, 2024)

Organic molecular ferroelectrics, including organic proton-transfer ferroelectrics and antiferroelectrics, are potentially attractive in organic electronics and have significant chemical tunability. Among these, acid-base proton transfer (PT) salts stand out due to their low coercive fields and the possibility to tune their properties with different acid-base combinations. Using crystal structure prediction, combining small acid and base organic molecular species, we here predict three novel acid-base PT ferroelectric salts with higher polarization than existing materials. We also report two combinations that form antiferroelectric crystal structures. However, some combinations also result in unfavorable packing or the formation of co-crystal or in one case a divalent salt. The protonation state is found to be highly linked to the crystal structure, with cases where salt crystal structures have the same energetic preferability as co-crystals with a different crystalline packing.

I. INTRODUCTION

There is growing interest in small-molecule ferroelectric and corresponding antiferroelectric materials.^{1–3} Traditional ceramic and polymer ferroelectrics find wide usage^{4,5} in capacitors, sensors, actuators, and memory devices,^{4,6} due to their piezoelectric and pyroelectric properties, along with their switchable spontaneous polarization (P_s).⁷ However, small-molecule variants offer potential advantages over ceramics such as biocompatibility,⁸ lightweight, low-cost fabrication routes, and integration into flexible substrates.^{1,3,9–12} Moreover, unlike standard polymer ferroelectrics that suffer from high coercive fields,^{10,13} they can host fast switching and low-voltage operation.^{14–16} A particularly attractive aspect of small-molecule ferroelectrics is the immense design flexibility offered through strategies such as functionalization^{17,18} and co-crystal engineering.^{19–21}

One type of organic small-molecule ferroelectrics is proton-transfer (PT) ferroelectrics, in which the polarization direction can be reversed through PT between molecules. Such systems can be realized both in tautomeric crystals,^{9,10,15,22,23} amphoteric compounds,²⁴ and in organic acid-base salts.^{25–29} Compared to the tautomeric crystals,¹⁰ the acid-base salts tend to have lower coercive fields, which can be of interest for low-energy switching and sensing.^{1,16} Designing novel acid-base PT salts with ferroelectric or antiferroelectric properties constitutes a significant co-crystal engineering challenge: changing the base or acid species—i.e., altering the size, shape, acidity, and functional groups—would allow for systematic adjustment of functional properties such as P_s , but can also change the preferred syn-

thetical hydrogen bonding³⁰ needed for PT switching. Moreover, it can also alter protonation states.³¹

Thus, it is essential to establish how robust the synths that support PT are to variations of the molecular species. The sensitivity to molecular species can be illustrated by the fact that replacing pyrazine in the bromanilic-pyrazine acid-base crystal³² with tetramethyl pyrazine changes not only the protonation state but also the hydrogen-bonding pattern.³³ So far only 10 acid-base PT ferroelectrics are known,^{21,25–28,34,35} limiting the amount of insight that can be gained from such comparisons. These systems all consist of derivatives of haloanilic acid combined with derivatives of phenazine, a tricyclic compound, or bipyridine, i.e., two linked pyridine rings,^{25–28} with PT between oxygen and nitrogen. Among these, the largest reported $P_s = 5.8 \mu\text{C}/\text{cm}^2$ is that of bromanilic and 2-(3-(pyridin-2-yl)pyrazin-2-yl)pyridinium salt²⁸ far lower than the value of the tautomeric compound croconic acid $P_s = 30 \mu\text{C}/\text{cm}^2$.¹⁵ Moreover, none of the 12 compounds uncovered in our recent screening study²⁹ of the Cambridge Structural Database (CSD) of known crystal structures,^{36,37} could be classified as acid-base PT salts. This scarcity of PT acid-base ferroelectrics highlights the need for targeted design of such compounds.

Crystal structure prediction (CSP) methods offer a systematic procedure to identify and assess the relative stability of the numerous possible three-dimensional crystalline arrangements of molecules or atoms from their basic constituents.^{38–40} Each of the local minima on the lattice energy surface is assumed to represent a possible stable crystal structure. CSP relies on efficient sampling methods, followed by local energy minimization to identify all relevant local minima. The predicted crystal structures are in turn ranked according to their relative calculated energies,^{41,42} with the resulting global energy minimum representing the most likely crystal structure to be observed. Due to the size of the search

* E-mail: kristian.berland@nmbu.no

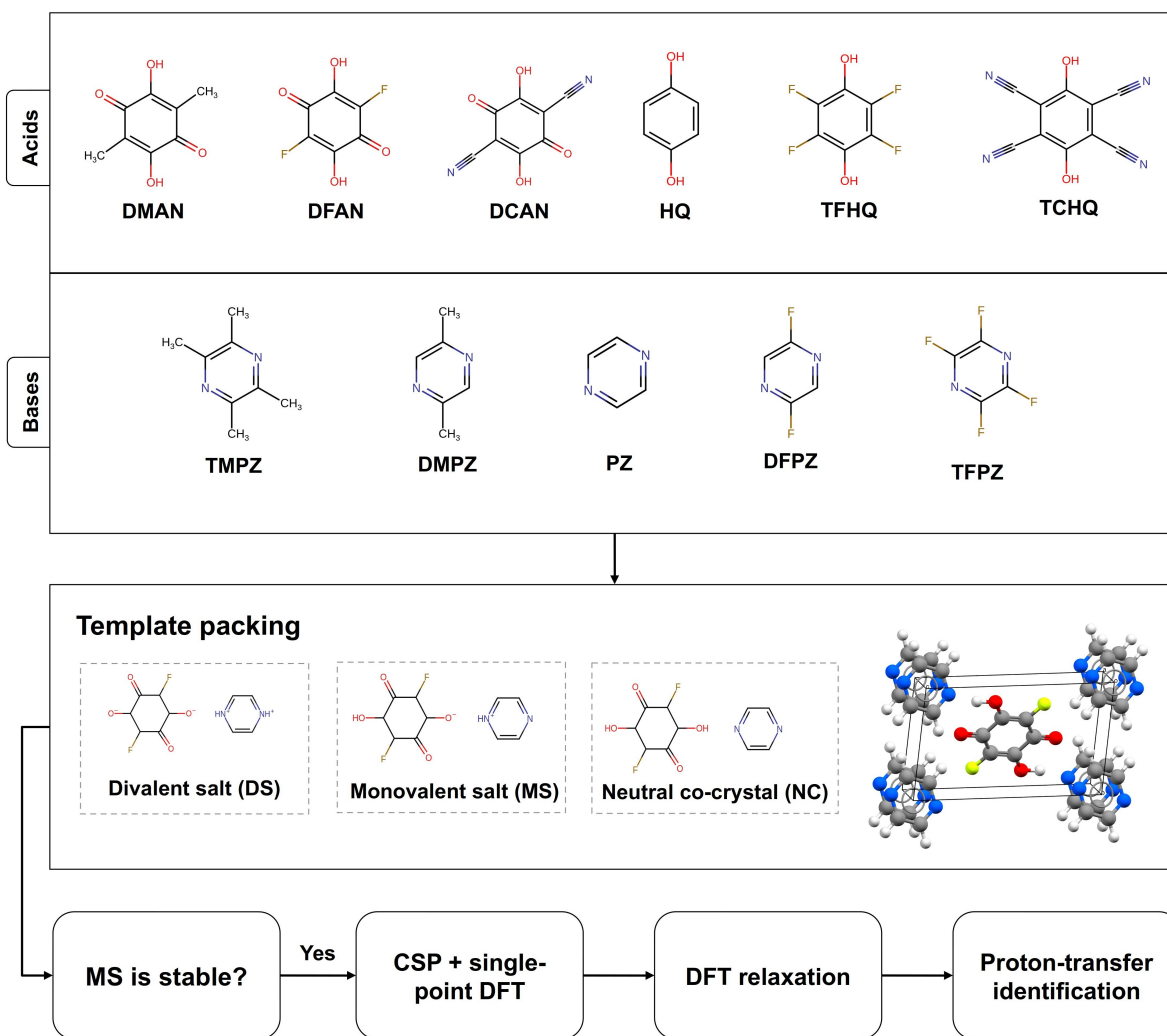


FIG. 1: The workflow of the acid-base PT salts design, showing the molecules studied (upper panel) and the summary of the computational screening strategy (lower panel).

space and the number of trial crystal structures that must be assessed, a preliminary CSP landscape is typically first generated with low-cost empirical or semiempirical force fields, limiting the number of systems that must be assessed with DFT.^{39,43} The success of the global optimization approach to CSP using these energy models has recently been assessed in a large-scale study,⁴⁴ demonstrating the reliability of the approach; 74% of the observed crystal structures for over 1000 molecules are located at, or within 0.02 eV of the global energy minimum from CSP. The reliability of CSP for molecular crystals can be further improved by applying higher-level ab initio methods, usually density functional theory (DFT) including dispersion corrections,^{45–49} to a limited number of low-energy structures.^{40,50}

CSP has been successfully applied in a growing number of studies to direct the discovery of new polymorphs, for example of pharmaceutical molecules,^{51,52} or to guide the functional material design.^{53,54}

In this paper, we present a CSP-based design of novel acid-base PT crystals. The approach is based on combining different pseudosymmetric single-ring molecular acid and base species that, with the right packing, could potentially support PT between nitrogen and oxygen. We only considered single-ring molecular species to increase the dipole density and enhance P_s . We also limited the scope to molecules with methyl, fluoro, cyano, and hydroxyl functional groups, thus totaling 30 combinations, i.e., 6 acids and 5 bases, as shown in the upper panel of Fig. 1, which describes the workflow of our study. Based on this screening, we predicted 3 novel ferroelectrics and 2 antiferroelectrics.

II. METHODS

A. CSP

The initial stage of crystal structure prediction was performed with rigid molecular geometries, which were optimized using DFT with the second version of the van der Waals density functional (vdW-DF2)^{45,55,56}, in a box with 15 Å of vacuum padding, using the electrostatic correction scheme of Neugebauer et al.⁵⁷. The configurational space of crystal structures was sampled using the Global Lattice Energy Explorer (GLEE) package,⁵⁸ which employs the Sobol quasi-random method⁵⁹ to uniformly sample molecular positions, orientations, and unit cell degrees of freedom. Unphysical structures with overlapping molecules were adjusted to relieve clashes, or rejected if clashes could not be relieved. Subsequent energy minimization of the trial crystal structures was performed using DMACRYS,⁴³ accounting for electrostatic interactions with atom-centered multipoles up to rank 4 and Buckingham-type atomistic potential with dispersion and repulsion terms implemented with interatomic parameters of the FIT potential.⁶⁰ Atomic multipoles were obtained from a distributed multipole analysis⁶¹ of the charge density obtained with the PSI4 software package⁶² at the B3LYP/6-311G** level.^{63,64}

The crystal structure search was performed over the ten most commonly observed space groups for co-crystals, P1, P $\bar{1}$, P2₁/c, C2/c, P2₁, P2₁2₁2₁, Pbc_a, Pna2₁, C2, and Cc, as well as the common space groups observed for PT ferroelectric crystals, P2/c, Pca2₁, Pnn2, Pccn, Fdd2, Iba2, P2, P3, P6₁, and I41/a.^{9,10,15,22,25-28} The criteria for terminating the quasi-random generation of crystal structures were either reaching 20,000 successfully energy-minimized structures per space group or failing to generate a new structure after a minimum of 100,000 attempts in that space group. Duplicate structures were removed from the final set of structures by evaluating the similarity of their simulated powder X-ray diffraction patterns generated with PLATON.⁶⁵ Comparison to experimentally determined crystal structures was also performed using COMPACK, counting the degree of similarity by the number of overlapping molecules within a 30 % distance and 30° angle tolerance threshold.

B. Density functional theory calculations

DFT calculations were performed with the projector augmented wave (PAW) approach, as implemented in the VASP software package.⁶⁶⁻⁶⁸ A plane-wave energy cutoff of 530 eV was used, which converged the energy difference per acid-base pair between two competing structures in the CSP to within 5 meV. As for the single molecules, vdW-DF2 was chosen since it could accurately predict the lattice parameters of earlier reported

organic PT ferroelectric crystals^{29,69} and different types of molecular crystals in more general.^{70,71} The Brillouin zone was sampled with a Γ -centered Monkhorst-Pack grid with a minimum k-spacing of (1/25) Å⁻¹. In the electronic optimization, self-consistency was reached when energy differences reached values below 10⁻⁸ eV. Ionic relaxations were performed until atomic forces fell below 0.01 eV/Å. Finally, the P_s values were computed using the Berry-phase method,⁷²⁻⁷⁴ by making a path to a centrosymmetric system using the procedure in Ref.²⁹ using the MOLCRYST Python tools.⁷⁵

III. RESULTS

A. CSP validation

To validate the ability to predict the experimental crystal structures of acid-base PT salts and associated protonation states, we first performed CSP for two systems with known crystal structures. The first, 2,3,5,6-tetrafluorobenzene-1,4-diol quinoxaline (CSD refcode: QUWZIS), is a hydrogen-bonded co-crystal with the P2₁2₁2₁ space group, which has the same packing as an acid-base salt, but with a neutral paraelectric co-crystal protonation state. The second, phenazinium chloranilate (CSD refcode: MAMPUM03),²⁶ is an acid-base PT salt crystallizing in the P2₁ space group below 254 K,³⁴ before transitioning to an analogous paraelectric phase. CSP was performed for both the neutral co-crystal and monovalent salt states to assess the ability to identify the correct protonation states.

Fig. 2 shows the CSP landscapes with the energy per acid-base combination plotted against the density. (a) and (b) show the results for molecular combinations with the experimentally favored QUWZIS, respectively, for single-point unrelaxed and relaxed DFT geometries. (c) and (d) show the corresponding for the MAMPUM03 acid-base salt. Comparing the unrelaxed and relaxed landscapes shows that the shift due to relaxation can be quite substantial.

For QUWZIS, a structure matching the experimental coincided with the global minimum single-point DFT energy, which after relaxation shifted to the second-ranked, but with almost the same energy as the lowest-ranked. Moreover, the lowest-ranked also has a rather high similarity to the experimental, nonpolar, and with identical hydrogen-bonding configurations. For MAMPUM03, a good match to the experimental study was also identified and ranked 20th in the single-point DFT landscape, but it dropped to the global minimum after relaxations. As for QUWZIS, the lowest competing low-energy structure also has a high similarity to the experimental one. The geometrical agreement between the matching CSP structure and the experimental structures is excellent; for QUWZIS, the 30-molecule overlay has a root-mean-square-deviation (RMSD) in atomic positions of 0.126 Å, which for MAMPUM03 (whose overlay

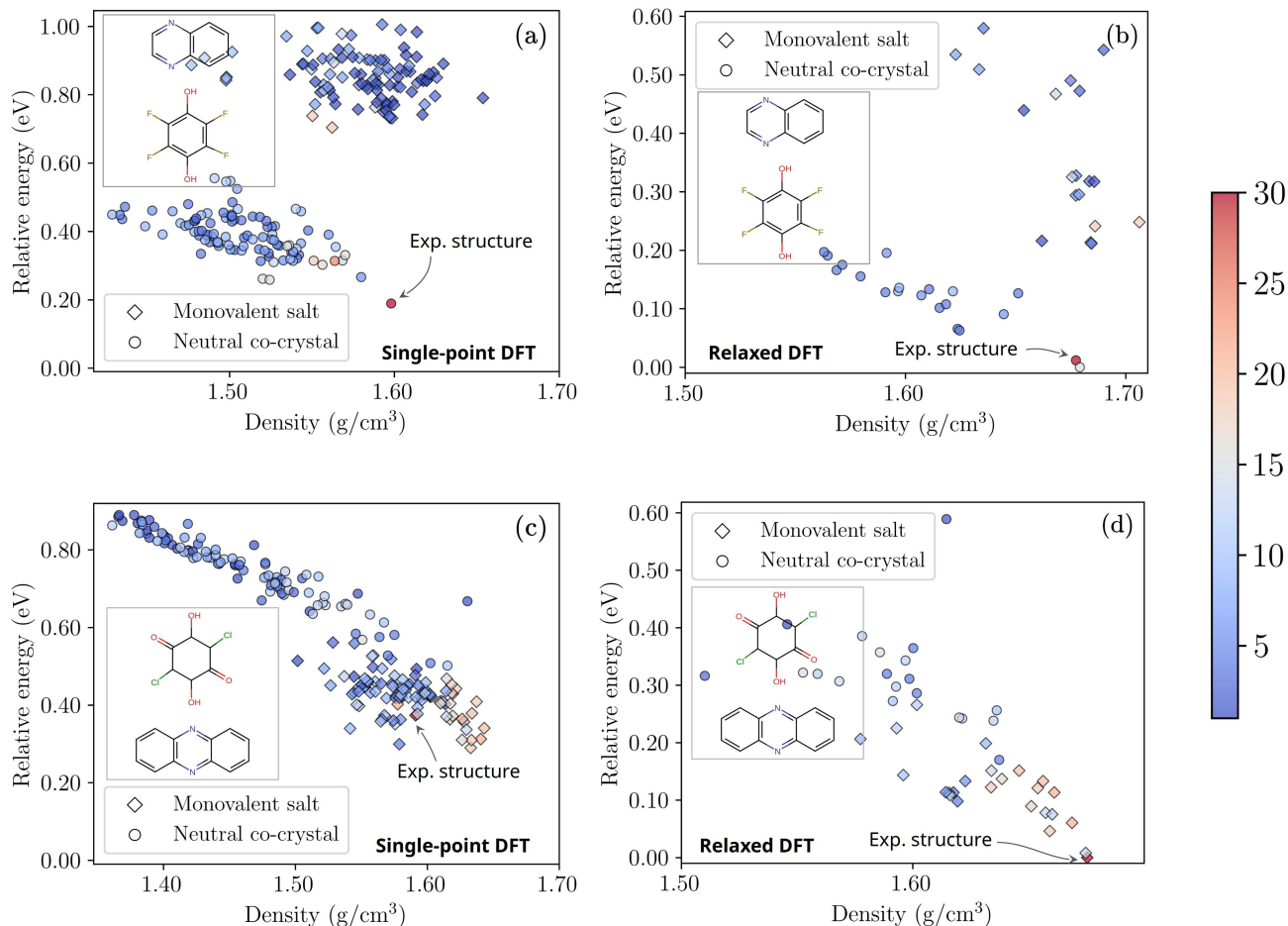


FIG. 2: The CSP landscapes for 2,3,5,6-tetrafluorobenzene-1,4-diol quinoxaline (upper panel) and phenazine chloranilate (lower panel) are plotted using single-point DFT (left) and relaxed DFT (right) energies. The colormap indicates the crystal structure similarity (number of matching molecules) to the experimental using COMPACK.

is shown in Fig. 3), the value is 0.217 Å.

The fact that CSP correctly predicted the experimental structure after relaxation for both validation systems as the lowest or almost so in the energy rankings after relaxation builds confidence in the ability to correctly predict additional acid-base crystal structures, including their protonation state. Correctly predicting protonation states at the DFT level is itself a highly challenging task due to limitations in current exchange-correlation functionals.^{76,77} We speculate that using non-local vdW-DF correlation, particularly vdW-DF2, can improve agreement with experimental results compared to DFT-D methods, due to their strong performance in our recent PT benchmark study⁷⁸

B. Co-crystal design

The design workflow is shown in Fig. 1. The following acids were considered: **Dimethyl anilic acid** (DMAN), **difluoro anilic acid** (DFAN), **dicyano**

anilic acid (DCAN), **hydroquinone** (HQ), **tetrafluoro hydroquinone** (TFHQ), and **tetracyano hydroquinone** (TCHQ); and the bases: **tetramethyl pyrazine** (TMPZ), **dimethyl pyrazine** (DMPZ), **pyrazine** (PZ), **difluoro pyrazine** (DFPZ), and **tetrafluoro pyrazine** (TFPZ).

In our study, a key criterion for PT ferroelectricity is the formation of an MS configuration. While PKa and similar criteria can provide some guidance, the protonation state of a molecule can be highly dependent on the environment. In an attempt to exclude some combinations without having to perform full CSP for all the structures, we first evaluated the protonation states in a relevant crystalline environment. For this purpose, we considered two different template packings, one of which is depicted in the “template packing” box in Fig. 1. To accommodate molecules with smaller functional groups such as DFAN, DCAN, PZ, and DFPZ, we adopted a tighter template arrangement with the P1 space group obtained from a similar compound (pyrazine chloranilic acid) deposited in CSD.⁷⁹ For systems with base species, a looser packing with the Pc space group from the CSP result of the largest

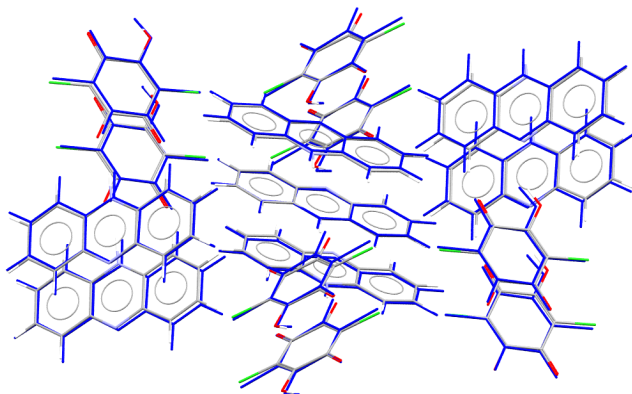


FIG. 3: Overlay of the CSP global energy minimum for phenazinium chloranilate (shown in blue) with the experimentally determined crystal structure, CSD reference code MAMPUM03 (shown with atoms coloured by element).

molecules (TCHQ-TMPZ) was employed.

Fig. 4 shows the resulting heatmap matrices of the energetic favorability of different protonation states. The upper panel shows the energy difference between the monovalent salt (MS) and neutral co-crystal (NC), or correspondingly the energy difference between the MS and divalent salt (DS) configurations, $E_{\text{DFT}}^{\text{MS}} - E_{\text{DFT}}^{\text{NC(DS)}}$, so that the blue-shaded regions indicate the favorability of the MS state. For several of the systems, we found the MS state to be dynamically unstable, which are marked by the X. With electron-withdrawing substituents, like the cyano group in DCAN and TCHQ, as well as bases with electron-donating groups like methyl in DMPZ and TMPZ, most of the blue shaded boxes in the upper panel appear in the lower right part. The lower panel shows that the molecular combinations with DCAN exhibit a tendency to donate both of their protons rather than just one, which is consistent with the fact that anilic acid rings tend to be more acidic compared to hydroquinone rings.^{80,81} In the full CSP evaluation, we retained 11 out of the 13 combinations exhibiting dynamically stable MS in the template crystal structures. The exceptions are DMAN-PZ, for which NC is more than 0.3 eV lower per acid-base pair than the MS salt and DCAN-TMPZ, for which DS is more than 0.3 eV lower than the MS salt. Initially, we planned to exclude more combinations based on the energetic favorability of the template packing, but initial CSP studies revealed a substantial impact of the crystal structure on the preferred protonation state, which is also in line with earlier studies.³¹ However, to limit the computational scope, we generally only performed CSP for the MS and NC protonation states. The exceptions are the cases where a ferroelectric or antiferroelectric packing are preferred in

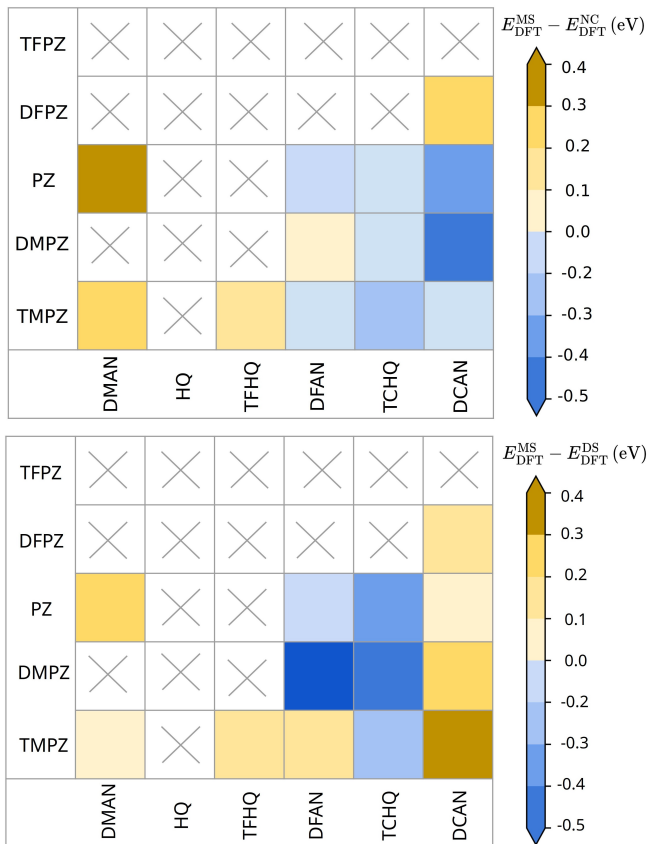


FIG. 4: In the upper panel, the energy difference of MS and NC contour is plotted for different molecular combinations. In the lower panel, the energy difference is plotted between MS and DS.

the global minimum and DS was preferred over MS in the template packing.

1. CSP using single-point DFT energies

Fig. 5 compares the energetic distribution of MS and NC crystal structures of the 100 lowest energy structures obtained from CSP with DMACRYS followed by a single-point DFT energy evaluation for the 11 considered combinations. For TFHQ-TMPZ and DCAN-DFPZ, most of the low-energy structures were NCs, with all MS structures having an energy of at least 0.2 eV above the optimal NC structure. Based on the validation study, in which both the single-point and relaxed DFT calculations correctly identified the protonation state, we deemed it unlikely that MS structures would become energetically favored with a DFT relaxation for these systems, and they were not examined further. NC was also preferred for DMAN-TMPZ, but in this case by such a small margin that it was retained for full relaxations. For all the others, MS was preferred, and they were retained.

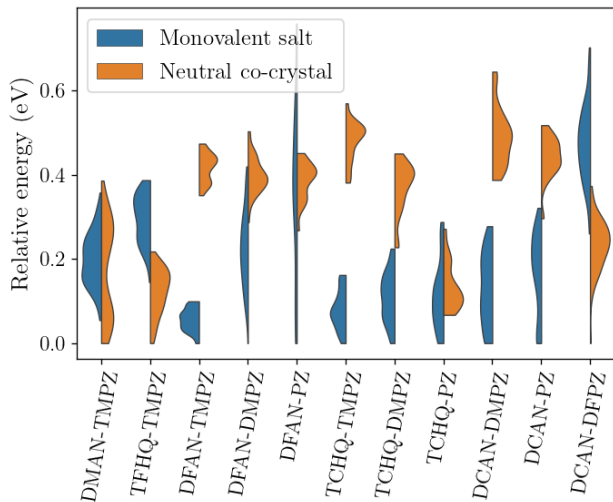


FIG. 5: Energy distribution of MS and NC structures generated by CSP using single-point DFT energies for the molecular combinations that successfully passed the template packing step.

Comparing the favored protonation state in the template packings in the upper panel of Fig. 4 with the energy distributions in Fig. 5 shows that the trends are generally maintained. However, for DFAN-DMPZ, an MS became preferred, which was also the one with the least energy difference between protonation states in the template packings. There is a significant overlap in the distribution of NC and MS structures in some cases, such as for DMAN-TMPZ, further highlighting the link between protonation state and crystal structure.

2. CSP using relaxed DFT energies

For four combinations of molecular species, we found global minima after DFT relaxations that were neither PT ferroelectric nor PT antiferroelectrics, as shown in Fig. 6. For both TCHQ-DMPZ (a) and TCHQ-PZ (b), a polar NC crystal structure was preferred with connected PT transfer paths. Such a structure can, in principle, be ferroelectric, but with a switching mechanism that is not PT. MS salts were also predicted, but none of them exhibited PT paths. In the lowest energy MS structures, the negatively charged side of TCHQ forms bonds with the positively charged side of the PZ or DMPZ species, while the neutral hydroxyl ($-OH$) group of TCHQ forms a bond with the cyano group of another TCHQ molecule. For DCAN-PZ (c) the global minima were MS structures without any PT connected path. For DCAN-PZ (d), there were no MS structures with connected PT paths among the relaxed structures, with more than 0.10 eV energy gap to the closest MS structure with a connected PT path. For this system, we

did not perform any CSP study for DS; however, since the template packing clearly favored such a configuration, we did relax the DS state of this molecular configuration and found it to be more stable than the MS state. As a result, we added the energy of the DS form of the structure in the global minimum to the landscape, which now represents the new global minimum. Other DS crystal structures with even lower energies might exist, but identifying these were not the target of our study.

Fig. 7 shows the CSP landscapes of DMAN-TMPZ (a) and DFAN-TMPZ (b) and the corresponding global minimum crystal structures. Both have MS global minima with connected PT paths, but nonpolar space groups. These conditions support PT antiferroelectricity. For DMAN-TMPZ, the antiferroelectric global minimum structure has a very small energy gap from a likely ferroelectric structure, while DFAN-TMPZ has a different antiferroelectric crystal structure as the second-ranked structure. For both these two structures, we performed CSP studies of the DS configurations at the single-point DFT level, since they were preferred in the template packings. However, we found the lowest energetic ones to be 0.7 eV and 1.7 eV above the preferred MS structures for DMAN-TMPZ and DFAN-TMPZ, respectively, and they were therefore not subsequently relaxed.

Fig. 8 shows the CSP landscape and selected associated crystal structures of DFAN-PZ (a), DFAN-DMPZ (b), and TCHQ-TMPZ (c). All three have global minima consistent with the conditions of PT ferroelectricity, i.e. MS with connected PT paths. For DFAN-PZ (a), most of the low-energy structures have connected PT paths, but many of them are also NC, and the closest structure is just 0.01 eV away from the global minimum. For DFAN-DMPZ (b) the closest is an antiferroelectric candidate, i.e., an MS with a centrosymmetric space group $P2_1/c$ and connected PT path. All low-energy structures for this combination were either potential ferroelectric or antiferroelectric crystals. For TCHQ-TMPZ (c), the low-energy region is mostly occupied by MS structures, but most of them do not have connected PT paths because of the extra synthons that come from the cyano side groups. Similar to the DFAN-PZ, the energy difference between the global minimum and the second-ranked exhibiting such a structure is merely 0.01 eV.

For the ferroelectric systems, we calculated $|P_s|$ to be 14.9, 15.0, and 9.1 $\mu\text{C}/\text{cm}^2$ for DFAN-PZ, DFAN-DMPZ, and TCHQ-TMPZ, respectively, with the first two having values nearly double those of existing acid-base co-crystals.

IV. CONCLUSION AND OUTLOOK

Using DFT and CSP, we evaluated 30 different combinations of acid and base molecular species to identify new acid-base PT salts with enhanced ferroelectric characteristics. In the preliminary stage, 18 combinations

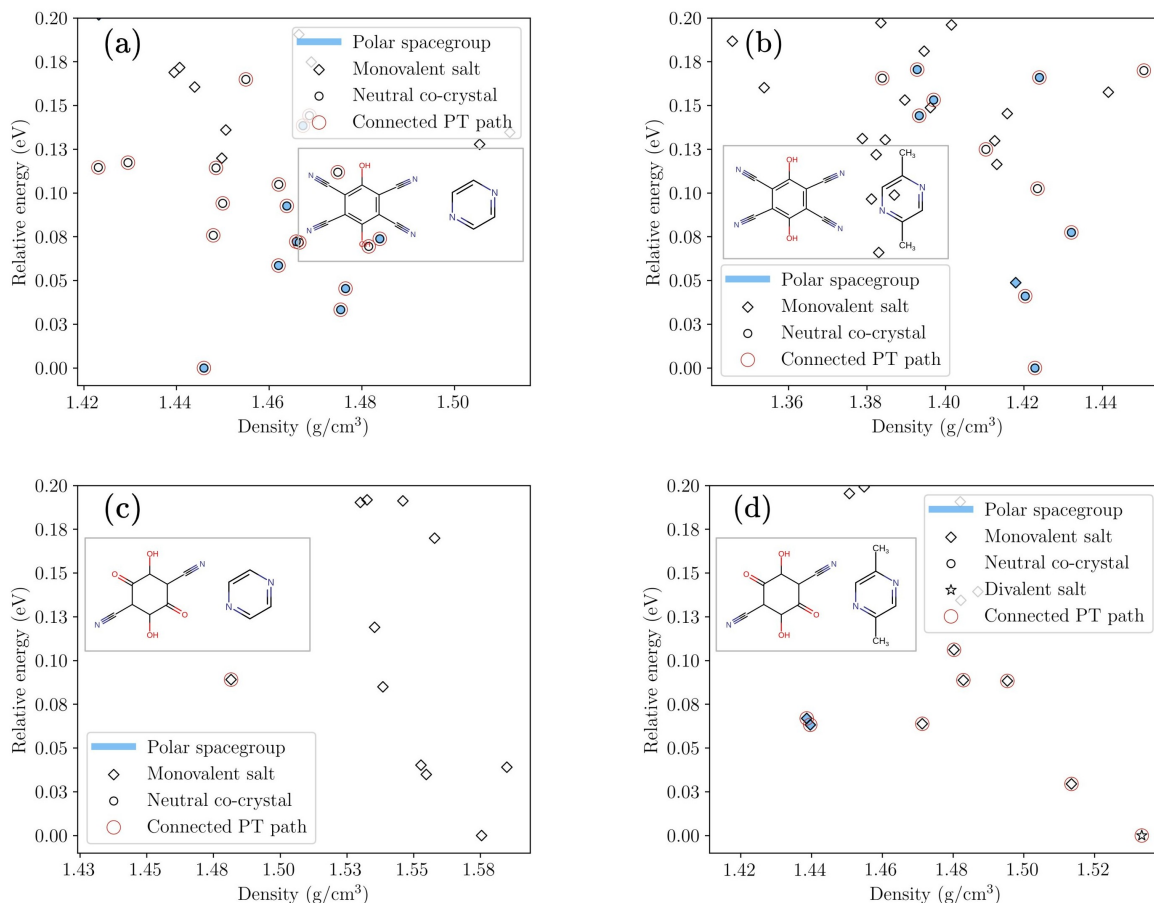


FIG. 6: The CSP landscapes for (a) TCHQ-PZ, (b) TCHQ-DMPZ, (c) DCAN-PZ, and (d) DCAN-DMPZ molecular combinations are plotted using relaxed structures DFT energies.

were ruled out due to the low favorability of the MS state. After the initial CSP analysis using DFT without relaxations, 3 more candidates were ruled out. Among the remaining 9, two exhibited antiferroelectric packing, and three exhibited ferroelectric packing.

Adding more electronegative groups to the acids and more electron-donating groups to the bases increased the prevalence of MS structures within the low-energy range. Increasing the acidity of acids and the basicity of bases can lead to a DS structure being the most stable, which was the case for one of the structures considered in our final CSP ranking. Although such considerations of acidity do provide guiding principles, as do considerations of synthon formation, i.e., functional groups in which new synthons emerge can more easily form structures without connected PT paths, our study highlights that many types of configurations including different protonation states can arise within the lowest energy structures. This finding highlights the crucial role of the unique environment of each crystal structure and hence also the importance of including CSP in the computational design of small-molecule organic ferroelectrics. CSP using DFT with the vdW-DF2 functional

was shown here to accurately predict the structure and protonation state of two validation systems with known structures.

Finally, we hope that the structures we have predicted ferroelectric - DFAN-PZ, DFAN-DMPZ, and TCHQ-TMPZ - will be realized and evaluated experimentally to test our predictions, or alternatively one of the systems predicted antiferroelectric

V. DATA AVAILABILITY

A dedicated GitLab page gitlab.com/m7582/csp_data describes generated data (with links to different NOMAD uploads), hosts python scripts used in data analysis and plotting, and describes the workflow for generating CSP landscapes. The complete NOMAD data set is provided at 10.17172/NOMAD/2024.10.22-1.

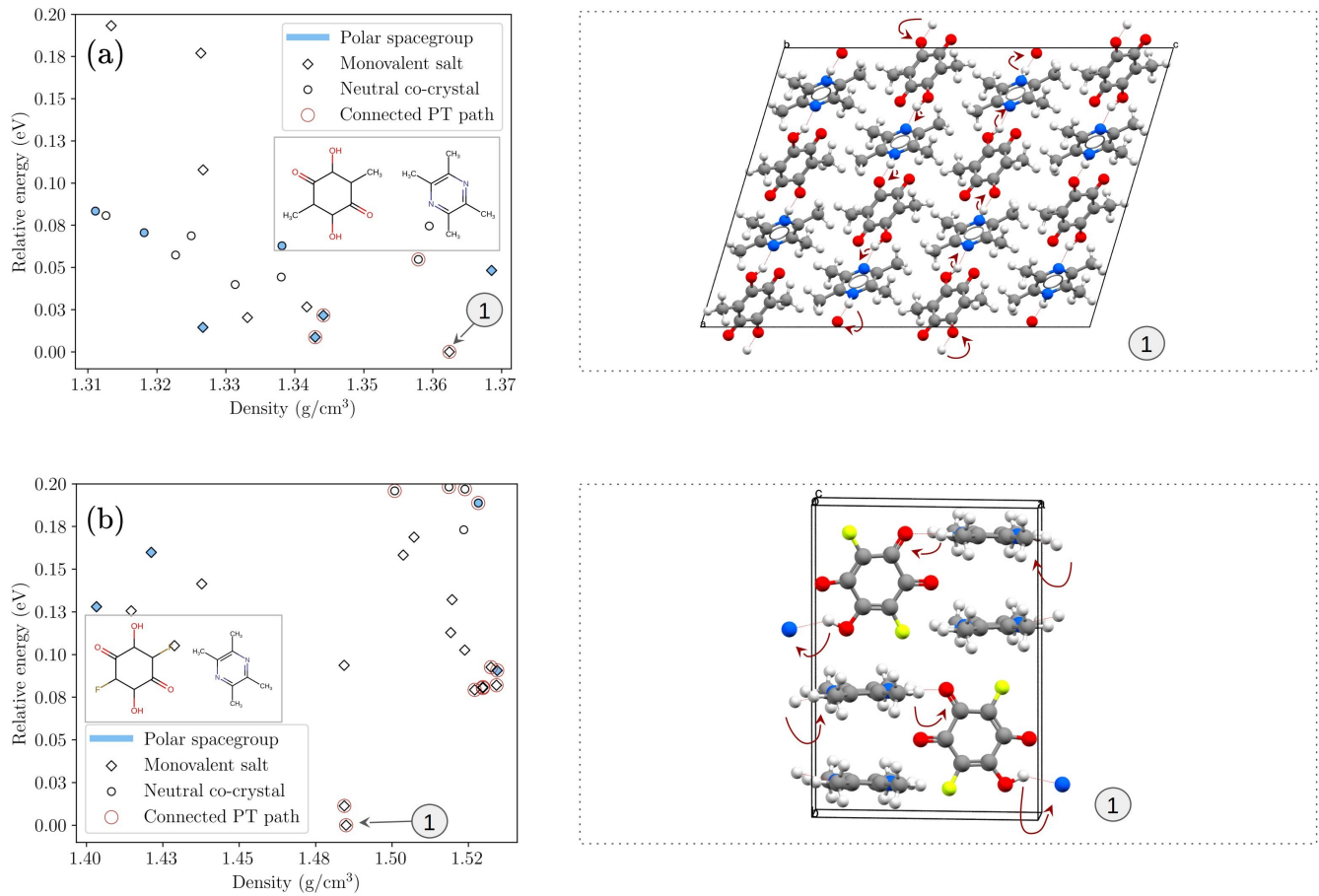


FIG. 7: The CSP landscapes for (a) DMAN-TMPZ and (b) DFAN-TMPZ molecular combinations are plotted using relaxed structures DFT energies.

ACKNOWLEDGMENTS

KB and SS acknowledge valuable discussions with O. Nilsen, C.H. Görbitz, and M. Balagopalan. The computations of this work were carried out on UNINETT

Sigma2 high-performance computing resources (grant NN9650K and NS8403K). Work by KB and SS is supported by the Research Council of Norway as a part of the Young Research Talent project FOX (302362). GMD thanks the European Research Council for funding, under the European Union's Horizon 2020 research and innovation program (grant agreement 856405).

- [1] S. Horiuchi, S. Ishibashi, and Y. Tokura, 3-hydrogen-bonded organic molecular ferroelectrics/antiferroelectrics, in *Organic Ferroelectric Materials and Applications*, Woodhead Publishing Series in Electronic and Optical Materials, edited by K. Asadi (Woodhead Publishing, 2022) pp. 47–84.
- [2] S. Horiuchi and S. Ishibashi, Hydrogen-Bonded Small-Molecular Crystals Yielding Strong Ferroelectric and Antiferroelectric Polarizations, *J. Phys. Soc. Jpn.* **89**, 051009 (2020).
- [3] Q. Pan, Z.-X. Gu, R.-J. Zhou, Z.-J. Feng, Y.-A. Xiong, T.-T. Sha, Y.-M. You, and R.-G. Xiong, The past 10 years of molecular ferroelectrics: Structures, design, and properties, *Chem. Soc. Rev.* **53**, 5781 (2024).
- [4] J. F. Scott, Applications of modern ferroelectrics, *Science* **315**, 954 (2007).
- [5] M. Mai, S. Ke, P. Lin, and X. Zeng, Ferroelectric polymer thin films for organic electronics, *J. Nanomater.* **2015**, 1–14 (2015).
- [6] J. F. Scott and C. A. P. de Araujo, Ferroelectric memories, *Science* **246**, 1400 (1989).
- [7] L. W. Martin and A. M. Rappe, Thin-film ferroelectric materials and their applications, *Nat. Rev. Mater.* **2**, 16078 (2016).
- [8] J. Li, Y. Liu, Y. Zhang, H.-L. Cai, and R.-G. Xiong, Molecular ferroelectrics: Where electronics meet biology, *Phys. Chem. Chem. Phys.* **15**, 20786 (2013).

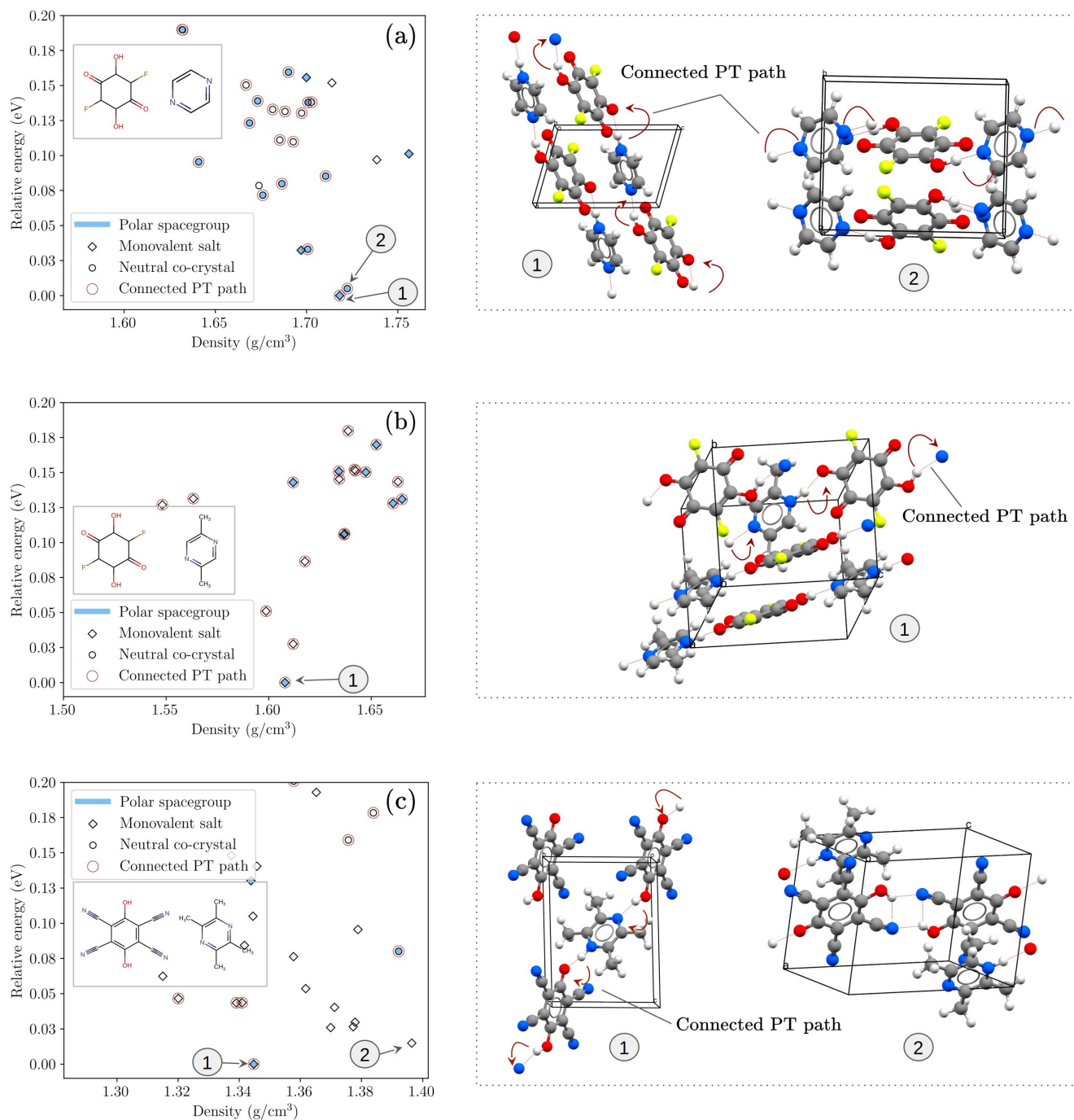


FIG. 8: The CSP landscapes for (a) DFAN-PZ and (b) DFAN-DMPZ (c) TCHQ-TMPZ molecular combinations are plotted using relaxed structures DFT energies.

- [9] S. Horiuchi et. al., Above-room-temperature ferroelectricity and antiferroelectricity in benzimidazoles, *Nat. Commun.* **3**, 1308 (2012).
- [10] S. Horiuchi, K. Kobayashi, R. Kumai, and S. Ishibashi, Proton tautomerism for strong polarization switching, *Nat. Commun.* **8**, 14426 (2017).
- [11] S. Horiuchi and Y. Tokura, Organic ferroelectrics, *Nat. Mater.* **7**, 357 (2008).
- [12] M. Owczarek et. al., Flexible ferroelectric organic crystals, *Nat. Commun.* **7**, 13108 (2016).
- [13] H. S. Choi et. al., Tailoring the coercive field in ferroelectric metal-free perovskites by hydrogen bonding, *Nat. Commun.* **13**, 794 (2022).
- [14] X.-J. Song et. al., Bistable state of protons for low-voltage memories, *J. Am. Chem. Soc.* **142**, 9000 (2020).

- [15] S. Horiuchi et. al., Above-room-temperature ferroelectricity in a single-component molecular crystal, *Nature* **463**, 789 (2010).
- [16] X.-J. Song, Z.-X. Zhang, X.-G. Chen, H.-Y. Zhang, Q. Pan, J. Yao, Y.-M. You, and R.-G. Xiong, Bistable State of Protons for Low-Voltage Memories, *J. Am. Chem. Soc.* **142**, 9000 (2020).
- [17] Y. Ai, H.-P. Lv, Z.-X. Wang, W.-Q. Liao, and R.-G. Xiong, H/F substitution for advanced molecular ferroelectrics, *Trends in Chemistry* **3**, 1088 (2021).
- [18] H.-Y. Liu, H.-Y. Zhang, X.-G. Chen, and R.-G. Xiong, Molecular Design Principles for Ferroelectrics: Ferroelectrochemistry, *J. Am. Chem. Soc.* **142**, 15205 (2020).
- [19] G. R. Krishna, R. Devarapalli, G. Lal, and C. M. Reddy, Mechanically flexible organic crystals achieved by introducing weak interactions in structure: Supramolecular shape synthons, *J. Am. Chem. Soc.* **138**, 13561 (2016).
- [20] X. Ding, C. Wei, L. Wang, J. Yang, W. Huang, Y. Chang, C. Ou, J. Lin, and W. Huang, Multicomponent flexible organic crystals, *SmartMat* **n/a**, e1213.
- [21] Y. Yamamura, E. Saito, H. Saitoh, N. Hoshino, and K. Saito, New Organic Ferroelectrics: Cocrystal of 5,5-Dimethyl-2,2-bipyridine and Bromanilic Acid, *Chem. Lett.* **41**, 119 (2011).
- [22] S. Horiuchi, R. Kumai, and Y. Tokura, Hydrogen-bonding molecular chains for high-temperature ferroelectricity, *Adv. Mater.* **23**, 2098 (2011).
- [23] S. Horiuchi, S. Ishibashi, R. Haruki, R. Kumai, S. Inada, and S. Aoyagi, Metaelectric multiphase transitions in a highly polarizable molecular crystal, *Chem. Sci.* **11**, 6183 (2020).
- [24] S. Horiuchi, Y. Noda, T. Hasegawa, F. Kagawa, and S. Ishibashi, Correlated proton transfer and ferroelectricity along alternating zwitterionic and nonzwitterionic anthranilic acid molecules, *Chem. Mater.* **27**, 6193 (2015).
- [25] S. Horiuchi, S. Ishibashi, K. Kobayashi, and R. Kumai, Coexistence of normal and inverse deuterium isotope effects in a phase-transition sequence of organic ferroelectrics, *RSC Adv.* **9**, 39662 (2019).
- [26] R. Kumai et. al., Structural assignment of polarization in hydrogen-bonded supramolecular ferroelectrics, *J. Am. Chem. Soc.* **129**, 12920 (2007).
- [27] S. Horiuchi, R. Kumai, and Y. Tokura, A supramolecular ferroelectric realized by collective proton transfer, *Angew. Chem. Int. Ed.* **46**, 3497 (2007).
- [28] S. Horiuchi, R. Kumai, and Y. Tokura, High-temperature and pressure-induced ferroelectricity in hydrogen-bonded supramolecular crystals of anilic acids and 2,3-di(2-pyridinyl)pyrazine, *J. Am. Chem. Soc.* **135**, 4492 (2013).
- [29] S. Seyedraoufi, E. D. Sødahl, C. H. Görbitz, and K. Berland, Database mining and first-principles assessment of organic proton-transfer ferroelectrics, *Phys. Rev. Mater.* **8**, 054413 (2024).
- [30] B. Sarma and B. Saikia, Hydrogen bond synthon competition in the stabilization of theophylline cocrystals, *CrystEngComm* **16**, 4753 (2014).
- [31] S. L. Childs, G. P. Stahly, and A. Park, The salt-cocrystal continuum: The influence of crystal structure on ionization state, *Mol. Pharmaceutics* **4**, 323 (2007).
- [32] M. Tomura and Y. Yamashita, One-dimensional supramolecular tapes in the co-crystals of 2,5-dibromo-3,6-dihydroxy-1,4-benzoquinone (bromanilic acid) with heterocyclic compounds containing a pyrazine ring unit, *CrystEngComm* **2**, 92 (2000).
- [33] K. Łuczynańska, K. Druzbicki, K. Lyczko, and W. Starosta, Complementary optical and neutron vibrational spectroscopy study of bromanilic acid: 2,3,5,6-tetramethylpyrazine (1:1) cocrystal, *Vib. Spectrosc.* **75**, 26 (2014).
- [34] S. Horiuchi, F. Ishii, R. Kumai, Y. Okimoto, H. Tachibana, N. Nagaosa, and Y. Tokura, Ferroelectricity near room temperature in co-crystals of nonpolar organic molecules, *Nat. Mater.* **4**, 163–166 (2005).
- [35] S. Horiuchi, R. Kumai, Y. Tokunaga, and Y. Tokura, Proton dynamics and room-temperature ferroelectricity in anilate salts with a proton sponge, *J. Am. Chem. Soc.* **130**, 13382 (2008).
- [36] C. R. Groom, I. J. Bruno, M. P. Lightfoot, and S. C. Ward, The Cambridge Structural Database, *Acta Crystallogr. B.* **72**, 171 (2016).
- [37] F. H. Allen, The Cambridge structural database: a quarter of a million crystal structures and rising, *Acta Crystallogr. B.* **58**, 380 (2002).
- [38] A. M. Reilly et. al., Report on the sixth blind test of organic crystal structure prediction methods, *Acta Crystallographica Section B* **72**, 439 (2016).
- [39] S. L. Price, Predicting crystal structures of organic compounds, *Chem. Soc. Rev.* **43**, 2098 (2014).
- [40] D. H. Bowskill, I. J. Sugden, S. Konstantinopoulos, C. S. Adjiman, and C. C. Pantelides, Crystal structure prediction methods for organic molecules: State of the art, *Annu. Rev. Chem. Biomol. Eng.* **12**, 593 (2021).
- [41] S. L. Price, Is zeroth order crystal structure prediction (csp0) coming to maturity? what should we aim for in an ideal crystal structure prediction code?, *Faraday Discuss.* **211**, 9 (2018).
- [42] S. M. Woodley, G. M. Day, and R. Catlow, Structure prediction of crystals, surfaces and nanoparticles, *Philos. Trans. R. Soc. A* **378**, 20190600 (2020).
- [43] S. L. Price, M. Leslie, G. W. A. Welch, M. Habgood, L. S. Price, P. G. Karamertzanis, and G. M. Day, Modelling organic crystal structures using distributed multipole and polarizability-based model intermolecular potentials, *Phys. Chem. Chem. Phys.* **12**, 8478 (2010).
- [44] C. Taylor, P. Butler, and G. M. Day, Predictive crystallography at scale: mapping, validating, and learning from 1,000 crystal energy landscapes, *Faraday Discuss.* , (2024).
- [45] K. Berland, V. R. Cooper, K. Lee, E. Schröder, T. Thonhauser, P. Hyldgaard, and B. I. Lundqvist, Van der Waals forces in density functional theory: A review of the vdW-DF method, *Rep. Prog. Phys.* **78**, 066501 (2015).
- [46] T. Thonhauser, S. Zuluaga, C. A. Arter, K. Berland, E. Schröder, and P. Hyldgaard, Spin signature of nonlocal correlation binding in metal-organic frameworks, *Phys. Rev. Lett.* **115**, 136402 (2015).
- [47] A. Tkatchenko and M. Scheffler, Accurate molecular van der Waals interactions from ground-state electron density and free-atom reference data, *Phys. Rev. Lett.* **102**, 073005 (2009).
- [48] S. Grimme, J. Antony, S. Ehrlich, and H. Krieg, A consistent and accurate *ab initio* parametrization of density functional dispersion correction (DFT-D) for the 94 elements H-Pu, *J. Chem. Phys.* **132**, 154104 (2010).
- [49] A. Otero-de-la-Roza and E. R. Johnson, A benchmark for non-covalent interactions in solids, *J. Chem. Phys.* **137**, 054103 (2012).

- [50] G. M. Day, Crystal structure prediction, in *Supramolecular Chemistry* (John Wiley & Sons, Ltd, 2012).
- [51] M. A. Neumann, J. van de Streek, F. P. A. Fabbiani, P. Hidber, and O. Grassmann, Combined crystal structure prediction and high-pressure crystallization in rational pharmaceutical polymorph screening, *Nat. Comm.* **6**, 7793 (2015).
- [52] C. R. Taylor, M. T. Mulvee, D. S. Perenyi, M. R. Probert, G. M. Day, and J. W. Steed, Minimizing polymorphic risk through cooperative computational and experimental exploration, *J. Am. Chem. Soc.* **142**, 16668 (2020).
- [53] A. Pulido, L. Chen, T. Kaczorowski, D. Holden, M. A. Little, S. Y. Chong, B. J. Slater, D. P. McMahon, B. Bonillo, C. J. Stackhouse, A. Stephenson, C. M. Kane, R. Clowes, T. Hasell, A. I. Cooper, and G. M. Day, Functional materials discovery using energy–structure–function maps, *Nature* **543**, 657 (2017).
- [54] M. O’Shaughnessy, J. Glover, R. Hafizi, M. Barhi, R. Clowes, S. Y. Chong, S. P. Argent, G. M. Day, and A. I. Cooper, Porous isoreticular non-metal organic frameworks, *Nature* **630**, 102 (2024).
- [55] K. Lee, E. D. Murray, L. Kong, B. I. Lundqvist, and D. C. Langreth, Higher-accuracy van der waals density functional, *Phys. Rev. B* **82**, 081101 (2010).
- [56] K. Berland, V. R. Cooper, K. Lee, E. Schröder, T. Thonhauser, P. Hyldgaard, and B. I. Lundqvist, “Van der waals forces in density functional theory: a review of the vdW-DF method”, *Rep. Prog. Phys.* **78**, 066501 (2015).
- [57] J. Neugebauer and M. Scheffler, Adsorbate-substrate and adsorbate-adsorbate interactions of Na and K adlayers on Al(111), *Phys. Rev. B* **46**, 16067 (1992).
- [58] D. H. Case, J. E. Campbell, P. J. Bygrave, and G. M. Day, Convergence properties of crystal structure prediction by quasi-random sampling, *J. Chem. Theory Comput.* **12**, 910 (2016).
- [59] I. Sobol’, On the distribution of points in a cube and the approximate evaluation of integrals, *USSR Comput. Math. & Math. Phys.* **7**, 86 (1967).
- [60] D. S. Coombes, S. L. Price, D. J. Willock, and M. Leslie, Role of electrostatic interactions in determining the crystal structures of polar organic molecules. a distributed multipole study, *J. Phys. Chem.* **100**, 7352 (1996).
- [61] A. Stone and M. Alderton, Distributed multipole analysis, *Mol. Phys.* **56**, 1047 (1985).
- [62] Daniel G. A. Smith et al., PSI4 1.4: Open-source software for high-throughput quantum chemistry, *J. Chem. Phys.* **152**, 184108 (2020).
- [63] A. D. Becke, “Density-functional thermochemistry. iii. the role of exact exchange”, *J. Chem. Phys.* **98**, 5648 (1993).
- [64] R. Krishnan, J. S. Binkley, R. Seeger, and J. A. Pople, Self-consistent molecular orbital methods. XX. A basis set for correlated wave functions, *J. Chem. Phys.* **72**, 650 (1980).
- [65] A. L. Spek, Single-crystal structure validation with the program *PLATON*, *J. Appl. Crystallogr.* **36**, 7 (2003).
- [66] G. Kresse and J. Hafner, Ab initio molecular dynamics for liquid metals, *Phys. Rev. B* **47**, 558 (1993).
- [67] G. Kresse and J. Furthmüller, Efficiency of ab-initio total energy calculations for metals and semiconductors using a plane-wave basis set, *Comput. Mater. Sci.* **6**, 15 (1996).
- [68] G. Kresse and J. Furthmüller, Efficient iterative schemes for ab initio total-energy calculations using a plane-wave basis set, *Phys. Rev. B* **54**, 11169 (1996).
- [69] K. Lee, B. Kolb, T. Thonhauser, D. Vanderbilt, and D. C. Langreth, Structure and energetics of a ferroelectric organic crystal of phenazine and chloranilic acid, *Phys. Rev. B* **86**, 104 (2012).
- [70] D. Chakraborty, K. Berland, and T. Thonhauser, Next-Generation Nonlocal van der Waals Density Functional, *J. Chem. Theory Comput.* **16**, 5893 (2020).
- [71] E. D. Sødahl, J. Walker, and K. Berland, Piezoelectric response of plastic ionic molecular crystals: Role of molecular rotation, *Cryst. Growth Des.* **23**, 729 (2023).
- [72] R. D. King-Smith and D. Vanderbilt, Theory of polarization of crystalline solids, *Phys. Rev. B* **47**, 1651 (1993).
- [73] R. Resta, Theory of the electric polarization in crystals, *Ferroelectr.* **136**, 51 (1992).
- [74] R. Resta, Macroscopic polarization in crystalline dielectrics: the geometric phase approach, *Rev. Mod. Phys.* **66**, 899 (1994).
- [75] K. Berland, E. D. Sødahl, and S. Seyedraoufi, *Molcrys*, <https://gitlab.com/m7582/molcrys/> (2023).
- [76] L. M. LeBlanc, S. G. Dale, C. R. Taylor, A. D. Becke, G. M. Day, and E. R. Johnson, Pervasive Delocalisation Error Causes Spurious Proton Transfer in Organic Acid–Base Co-Crystals, *Angewandte Chemie* **130**, 15122 (2018).
- [77] Y. A. Abramov and J. Wang, Is It Salt, Cocrystal, or Continuum? Successes and Limitations of Computationally Efficient Periodic System Calculations, *Crystal Growth & Design* **24**, 4017 (2024).
- [78] S. Seyedraoufi and K. Berland, Improved proton-transfer barriers with van der waals density functionals: Role of repulsive non-local correlation, *J. Chem. Phys.* **156**, 244106 (2022).
- [79] H. Liu, M. J. Gutmann, H. T. Stokes, B. J. Campbell, I. R. Evans, and J. S. O. Evans, Supercolossal uniaxial negative thermal expansion in chloranilic acid pyrazine, *ca-pyz*, *Chem. Mater.* **31**, 4514–4523 (2019).
- [80] R. N. Beale and A. Liberman, 469. the determination of the dissociation constants of very sparingly soluble weak electrolytes, *J. Chem. Soc.*, 2287 (1950).
- [81] S. I. Mostafa, Complexes of 2,5-dihydroxy-1,4-benzoquinone and chloranilic acid with second and third row transition elements, *Transit. Met. Chem.* **24**, 306–310 (1999).